 DOI: 10.1002/maco.201408115

Soil-induced corrosion of ancient Roman brass – A case study

O. Papadopoulou*, P. Vassiliou, S. Grassini, E. Angelini and V. Gouda

This work focuses on the study of the solid state processes on naturally corroded ancient brass artefact. The object, recovered from burial in the Tiber riverbed in Italy, has been characterised from a morphological, chemical and microstructural point of view. The artefact probably originates from a Roman brass coin or medal and the alloy substrate was identified as a leaded brass (85% copper, 12.8% zinc and 2.2% lead). A combination of XRF, SEM coupled with EDS spot analyses and elemental mapping, Raman spectroscopy and OM observations were employed in order to describe the corrosion processes that created the heterogeneous, multi-layer corrosion product stratification. The identification of copper sulphide layers and the precipitation of some, rarely reported, basic copper and zinc phosphates are among the most important findings of this work. Two phases of anaerobic and aerobic corrosion emerged from the analyses. The object has undergone dezincification at early stages and decuprification later on. However, the most crucial action was the environmental elements activity, which determined the corrosion rate and the nature of the corrosion product layers. The results are critically discussed and correlated with the environmental conditions of the burial context. The study is supported by an extensive literature review.

1 Introduction

Alloy chemical composition, microstructural features and corrosion layer stratification provide archaeologists, researchers and conservators with scientific evidence, necessary for dating, authentication and identification of historical and cultural origin of archaeological metal findings. Moreover, the understanding of complex corrosion mechanisms - electrochemical and chemical - is a fundamental prerequisite for the development of sustainable stabilization and conservation procedures for cultural heritage metal objects.

O. Papadopoulou, P. Vassiliou
Lab of Physical Chemistry, School of Chemical Engineering, National Technical University of Athens, 9 Iroon Polytechniou str., 15780, Athens, Greece
E-mail: olpap@central.ntua.gr

S. Grassini, E. Angelini
Department of Applied Science and Technology, Politecnico di Torino, Corso Duca degli Abruzzi 24, 10129 Torino, Italy

V. Gouda
National Research Center, Cairo, Egypt

The preservation state, at which the metal artefacts are encountered, varies according to their chemical composition, the particular metalworking practice employed during manufacturing, the exposure period and most important the effect and fluctuation of numerous environmental parameters such as pH, oxygen supply, presence of marine, urban or agricultural corrosive agents, temperature and moisture cycles. The sequence of the undergoing corrosion processes, very often produces a natural composite material constituted of a metal core and mineral compounds. The corrosion process leads to the deposition of insoluble compounds in crevices of the original surface and in the form of successive layers, most of the times irregular and disrupted [1,2]. The survey research of *Robbiola* et al. [3] on bronzes recovered from burial conditions resulted in the classification of the corroded surfaces in two main types (Type I and II). The two corresponding corrosion mechanisms are described in terms of solid state migration of both alloying and environmental elements. The process can either be controlled by the metal cation diffusion outwards, or by the corrosive anion penetration towards the alloy interface. In case of binary copper-tin bronzes a selective dissolution of copper (decuprification) is observed [3].

Copper-zinc binary alloys (brasses) with high amounts of zinc may become destabilized and lose the alloying element.

Dezincification of brass is considered to occur by one of two alternative mechanisms: (a) dissolution of both zinc and copper in the brass, followed by redeposition of copper or (b) selective dissolution of the zinc leaving the copper behind [4]. Brasses with a zinc content over 15% weight are susceptible to dezincification, but this rule may not pertain to ancient specimens due to casting segregation [1]. It is important to clarify that decuprification mechanism, in contrast with zinc preferential dissolution due to galvanic corrosion of the alloy, is based on the transportation of cation vacancies from the bulk to the electrolyte (i.e. the soil).

Copper alloys are also vulnerable to biological corrosion. Micro-organisms within the biofilm are capable of maintaining an environment at the surface of the artefact that is radically different from the bulk in terms of pH, dissolved oxygen and other organic and inorganic species. Differential aeration, selective leaching, underdeposit corrosion and cathodic depolarisation have been reported as mechanisms for microbiologically influenced corrosion of copper alloys. *Little* et al. have published several reports on the biofilm reactions on metal surfaces and the correlation of micro-organisms activity with the evolution of particular corrosion products [5]. Copper alloys, in general prevent or retard the settlement of macrofouling species such as barnacles and mussels. However, bacteria, microalgae, protozoa and their cellular exudates form a slime layer on copper containing surfaces [5]. Copper sulphides are related to the activity of sulphate reducing bacteria in anaerobic environments – their principal habitats are soil, sediments and seawater [6]. The impact of phosphorus cycle in the concentration of phosphates in soil is described in [7]. The main sources of phosphorus are the weathering of primary and secondary minerals and the washing out of fertilizers from agricultural areas. Phosphorus also originates from the decomposition of organic matter and enters the phosphorus cycle through the mechanisms of mineralization and immobilization. Orthophosphates is the most common soluble form of phosphates. When the pH is higher than 7, monohydrogen phosphate is the form that predominates. There are several factors affecting the sorption of phosphorus from the soil and its solubility and precipitation as well. Regarding the ancient bronzes and early brasses, many case studies of long-term natural corrosion, as well as accelerated corrosion experiments and electrochemical investigations, have been published in the past, relating alloying elements and environmental corrosive agents with particular corrosion patterns [1,3,8–17]. Recent studies on ancient iron, have proposed new methodologies for the understanding of ancient metals corrosion mechanisms, involving both thermodynamic data based on on-site monitoring of the environmental conditions and laboratory corrosion tests [18]. Unfortunately, this practice cannot be applied to all excavated objects. Thus, the proposition of a detailed corrosion mechanism in most of the cases is subjected to several limitations.

The burial context of interest, related to this study is briefly described. Tiber riverbanks, in Rome, are surrounded by several volcanic complexes that form part of the Roman Magmatic Province located in Central Italy, in the province of Lazio. The volcanic activity of the region is related with the presence of igneous rocks and post-eruptive sediments in the basin and banks of river Tiber [19]. Tiber, because of its location in a densely populated area, is among the large rivers that still suffer from organic pollution despite the intensification of domestic and industrial waste water biological treatment during the last 35-40 years. After World War II, discharge of organic waste into surface waters increased in many European countries with resultant severe oxygen depletion. In European rivers in particular, the load of phosphate and nitrate fertilizers that end up in surface waters has also increased with a significant impact in river biogeochemistry [20]. On-site monitoring data collected at downstream stations of Tiber river for the period 1990-1992, allow an estimation of the environmental parameters which determined the more recent 'corrosion history' of the corroded metal artefact [21].

In the field of historical research on ancient metallurgy, the deliberate systematic production of brass takes place in Roman times. Although initially restricted to coin production, during the 1st and 2nd centuries AD the use of brass became popular in other fields, especially decorative metalwork where it largely replaced bronze. Since the cementation process had been established in the Roman Empire brass had the obvious advantage of cheapness - its price was about one-tenth of the price of tin and only half the price of copper - and was much more abundant than tin, especially for large scale metal production such as coinage [22]. *Craddock* in his studies [22] divides the Roman brasses into three representative categories according to their zinc content. The first group contains less than 4% zinc and the presence of zinc almost certainly arises from the use of scrap brass in the alloy. The second group contains between 4 and 20% zinc with an essentially normal distribution around 13%. It is assumed that these alloys were produced by mixing freshly made brass containing 22 to 28% zinc with scrap bronze. The brasses of the third group are produced straight from the smelter, without the addition of any scrap bronze or copper to reduce the overall zinc content; their zinc content lies between 22 and 28%.

In this work, the historical origin, authentication and use of the particular metal object, as well as the corrosion phenomena resulted in its present condition are under investigation.

2 Experimental

2.1 Metal sample documentation and evidence of the burial context

In the framework of the EFESTUS project (funded by the European Commission, contract No. ICA3-CT-2002-10030), a large number of archaeological bronze artefacts from the Mediterranean basin were studied [23]. The aim was to investigate the corrosion of bronze archaeological artefacts with widely different cultural and geographical origins. Some unusual corrosion case studies of the objects examined have been published [24].

Several artefacts have been found along the riverbanks of Tiber, in Italy, during cleaning activities. Some of them were selected for analysis. The metallic fragment (named *art1*) is among the items not analyzed during the European program. It is part of an artefact of unknown chemical composition. Like all items upon finding, it was closed in airtight plastic bag and

stored in controlled environment in the laboratory. Due to the well-crystallised patina, the environmental effects on the post-burial condition are considered minimal. Before the analyses, the fragment was photographed as received (free from soil residues) and its initial dimensions were recorded (Fig. 1). The documentation was also accompanied by macroscopic observations.

During the EFESTUS program, soil samples have been collected from the burial context and several physical and chemical analyses were performed. In this work, the most relevant data will be presented along with the results.

2.2 Sample preparation and analytical methods

The artefact bulk analysis was performed by X-ray fluoresence (XRF) using a Thermo ARL ADVANT XP sequential spectrometer. The surface morphology was observed by means of a FEI QUANTA 200 scanning electron microscope (SEM) equipped with a tungsten filament and solid state back scattered electron detector. The instrument is coupled with energy dispersive spectroscopy (EDS) for elemental analysis. The cross-section was prepared by grinding with silicon carbide abrasive papers ranging from 400 up to 2000 grit and polishing, with diamond pastes and alcohol-based lubricant, until a mirror-like surface was achieved. Then, the polished surface was cleaned in ethanol in an ultrasonic bath for few minutes to remove the residual abrasive particles. A detailed morphological characterization was performed by SEM and EDS was employed for spot chemical analyses on the corrosion layers and element mapping for copper, zinc, oxygen, sulphur, phosphorus, chlorine, potassium, silicon, calcium and aluminum. The accelerating voltage of the electron beam was set at 25 kV. 50 frames were acquired for the element maps. Optical microscopy observations (in bright field and under polarized light) were carried out using a Leitz Aristomet metallographic microscope in order to study the morphology of the corrosion layer stratification. SEM and OM pictures were taken before and after the cross-section preparation, to ensure that mineral phases vulnerable to thermo-mechanical alteration during grinding, if present, could be depicted [1]. Raman spectra were obtained with a Renishaw Ramascope RM1000® Raman micro-spectrometer. Spectra were excited at room temperature with the 632.8 nm line of a red 19 mW He-Ne laser through an OLYMPUS® x50 objective. The numerical aperture of the objective is 0.9. The laser spot on the surface has a diameter of approximately 1 μm and a power of 4 mW. The entrance slit into the spectrometer was set to 40 μm. Light was dispersed by a holographic grating with 1800 grooves/mm. The "scanning" mode was selected in order to avoid step-like mismatches between neighbouring spectral windows that often occur with samples with intense and uneven background and several successive acquisitions. Three accumulations of 20 seconds each were made to provide a good signal-to-noise ratio (*Knoll* et al. 1990). Wavenumber calibration was checked regularly by measuring the position of the Rayleigh line and the LO phonon mode of a silicon single crystal wafer.

The metallographic characteristics of *art1* were studied after colour etching with Klemm's II reagent, which is suitable for α-brasses. The specimen was immersed for 6 minutes in the tint etching solution and afterwards, was washed in warm deionized water, rinsed with ethanol and dried [25].

3 Results and discussion

3.1 Object origin and history – A proposed possible scenario

The estimated chemical composition of *art1* metal core is 85% copper, 12.8% zinc and 2.2% lead. Silver, iron and sulphur were detected as minor inclusions.

The alloy chemical composition, the fragment shape and calculated diameter, along with the data collected from a literature review, lead to the assumption that it could probably be a part of a brass sestertius (or of another large brass coin) struck between the first three Centuries of the Roman Empire (1^{st} - 3^{rd} century AD).

The measured metal core thickness (4.5 - 6 mm), on the other hand, exceeds the typical sestertius thickness, which is usually about 4 mm thick. Thus, the case of being a medal of the same period cannot be excluded. Moreover, since the zinc content is about 12%, *art1* falls into the second brass category, according to the *Craddock* classification [22]. The absence of tin and the presence of 2.2% lead raise some other interesting issues. The archaeological studies show that tin and most of the lead were usually introduced from the scrap metal added to the original brass. However, according to [22], the Imperial coiners and Legionary smiths of the 1^{st} and 2^{nd} century AD usually used pure copper to dilute the brass, instead of scrap bronze generally employed by small commercial producers. These considerations lead to think that *art1* could really be a fragment of an ancient coin. Finally, the lead amount could be added deliberately to

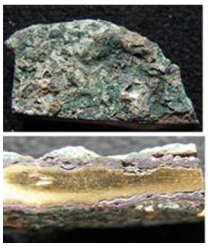

Maximum Length (mm)	Maximum Width (mm)	Average Total Thickness (mm)	Max Patina Thickness (mm)
23	10	8	1.5

Figure 1. Art1 photographic documentation and dimensions.

Table 1. Particle size distribution of soil samples from burial context - Calculated mean values and standard deviation of the % weight fractions after sedimentation of two initial 10 g samples of soil collected from Tiber riverbanks.

Clay (<0,002 mm)	Fine lime (0.002-0.02 mm)	Coarse lime (0.02-0.05 mm)	Fine sand (0.05-0.2 mm)	Coarse sand (0.2-2 mm)
11.63 ± 0.13	18.00 ± 0.95	4.25 ± 0.35	44.3 ± 0.5	21.83 ± 0.93

improve the alloy working properties or its presence could be due to the copper ore minerals or to casting impurities.

3.2 Soil analyses

The texture of the collected soil samples is sandy loam with a pH of 8.3. The particle size distribution of the soil samples collected from the excavation site are presented in Table 1. The results of soil analysis are given in Table 2. The electrical conductivity was 602 µS/cm. These measurements are in good agreement with earlier bibliographic data reported in [21].

3.3 Investigation of natural corrosion processes

3.3.1 General observations

Art1 is characterized by a complex and heterogeneous corrosion products layer stratification. The still present large metal core is externally covered by a dark green, coarse, mineralized crust of irregular thickness. Many incorporated soil crystals are visible in the patina, whose thickness reaches the maximum value of 1.5 mm in some points.

3.3.2 Cross-section analysis

The metallographic examination after colour etching revealed the manufacture history of *art1* (Fig. 2a). The observed twins and the grain size variation – the grain size decreases towards the metal/patina interfaces – indicates initial cold work after casting. Afterwards, the alloy has been annealed and subsequently, the object was 'heavily' cold worked. The twins and grain boundaries are distorted by slip lines. At the interfaces, the object has undergone dealloying. In these zones, the observation of elongated crystals with slip deformation is more pronounced. In the metal core, on the other hand, the well recrystallized grains are better maintained.

These metallurgical features are typical of coins and medals, so the previous hypothesis seems to be confirmed.

The corrosion stratification above metal is constituted by three main (not everywhere clearly distinguished) corrosion layers. According to the terminology proposed by *Neff* et al. [26]:

Table 2. Results of soil analysis – weight concentrations of nitrogen, carbon and phosphorus.

% Nitrogen	% Carbonates	% Organic carbon	% Total carbon	Total phosphorus (ppm)
0.4	2.0	0.8	2.8	1.4

(a) the first layer is a dense product layer (DPL) adhered to the metal, 600 to 900 µm thick, (b) the second layer is the transformed medium (TM), with a thickness ranging from 350 µm to 1 mm, which is rich in elements from burial context and has incorporated soil particles and (c) the outer layer is a "earthy" crust with irregular thickness in the range of 0 to 400 µm, which is mainly composed by insoluble precipitates, while the concentrations of alloying elements are extremely low.

Some very interesting remarks derive from the examination of the corrosion layer morphology and chemical composition from the bulk towards the surface. The corroded slip lines and the presence of a thick, coherent cuprous oxide (cuprite) layer next to the metal surface (Fig. 3a) are also evidence of authenticity of the ancient object [2]. It must be noted that zinc loss is already remarkable in this first dealloyed zone (dz), where the zinc content is reduced to half of the initial alloy concentration (Table 3).

The preferential dissolution of zinc (dezincification) is more pronounced towards the first corrosion layers. The zinc depletion zone is also clearly located by mapping (Fig. 4). A thin black layer (Fig. 2b), probably cupric oxide (tenorite) according to the EDS relative elemental concentrations (Fig. 3a, spot 1 - Table 4), is followed by a compact red cuprite layer (Fig. 3a, spot 2 - Table 4). A second black layer, which appears compact in some areas (Fig. 2b) and porous and fragmented in other points, is found right above. This layer could either be related to an original decorative patination of the brass with niello (a mixture of copper, silver and sometimes lead sulphides) [1,22] or could have been formed under anaerobic conditions in the areas rich in sulphate reducing bacteria (during burial or in stagnant conditions such as lakes, river sediments or hot springs).

This pattern is one of main characteristics of '*lake patinas*' according to *Schweizer* (1994) [8] and to several other interesting cases reviewed by *Scott* in [1]. Fig. 3b shows a part of this fragmented black crust, which is composed by 26.9% sulphur, 58.8% copper, carbon and a low content of oxygen (spot 3 - Table 4). Neither silver nor lead was traced, which means that the hypothesis of deliberate patination with niello is rejected. On the other hand, the stagnant conditions inside the river sediments, enriched in organic matter could benefit anaerobic biological activities. Copper sulphides generally vary widely in composition and several non-stoichiometric compounds, characterised by a copper/sulphur ratio ranging between 0.5 and 2, can be formed. In correspondence to the black crust (Fig. 3b, spot 3 - Table 4) the copper/sulphur atomic ratio is 2.2, very close to the stoichiometry of chalcocite. According to [5], the possible corrosion reactions in a copper sulphide system are extremely complex because of the large number of stable copper sulphides, their differing electrical conductivities and catalytic effects. The characteristic 'spongy' structure and a huge gap (visible even macroscopically), are

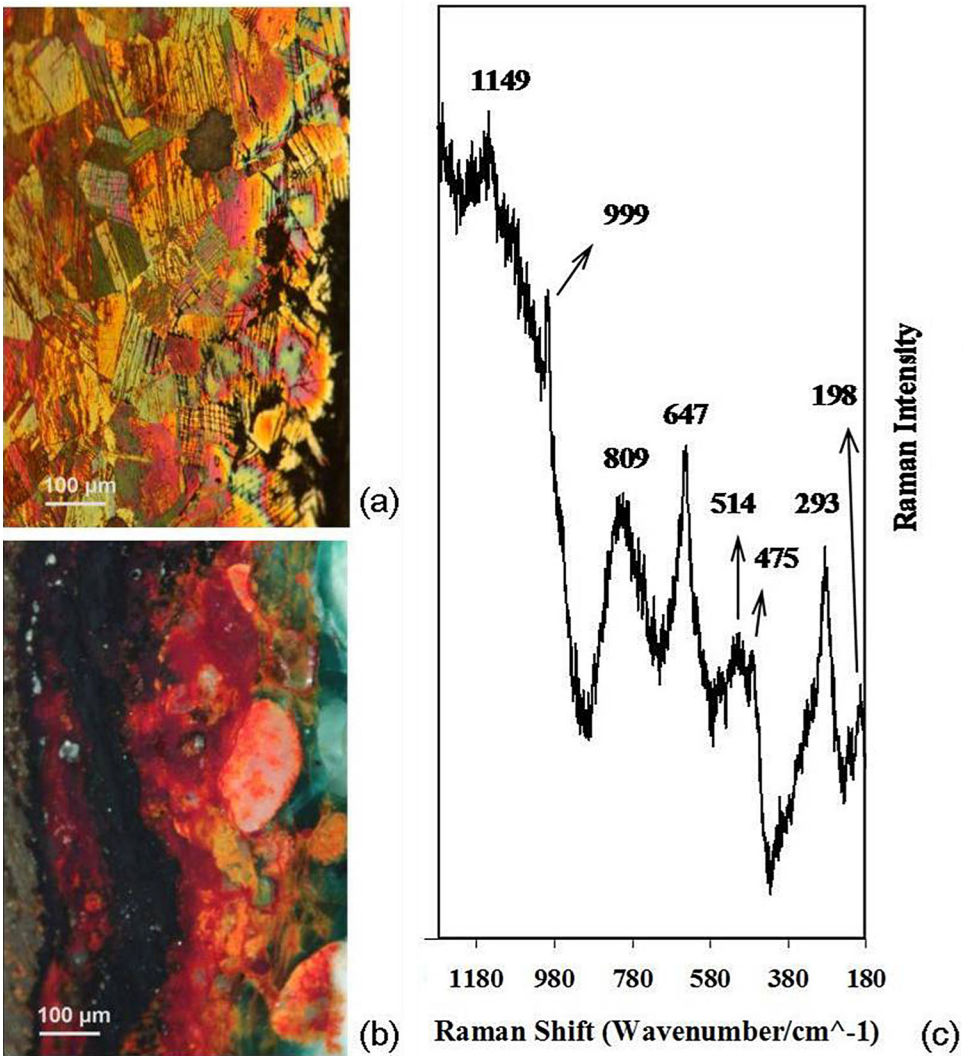

Figure 2. (a) Metallographic features of the alloy near the metal/patina interface highlighted by colour etching with Klemm's II reagent, (b) x100 OM image of art1 cross-section under polarized light, (c) low wavenumber region of Raman spectrum collected from the vitreous bluish-green phosphate corrosion compounds – possibly attributed to $Cu_5(PO_4)_2(OH)_4$ species.

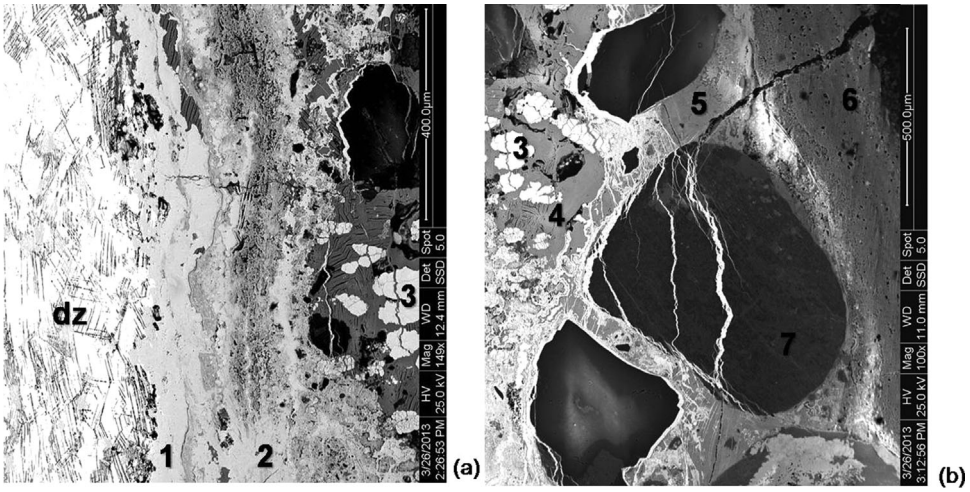

Figure 3. SEM backscattered electron images of art1 cross-section after polishing: (a) x149 and (b) x100.

Table 3. Calculated atomic percentages derived from EDS data corresponding to the numbered spots presented in Fig. 3a, 3b and the alloy substrate.

	Bulk alloy	Dealloyed zone (dz)	1	2	4	5	6	Surface
Environmental elements (%)	–	47.7	46.5	36.5	72.5	83.9	93.8	87.0
Alloying elements (%)	100	52.3	53.5	63.5	27.5	16.1	6.2	13.0
Cu/Total metals (%)	85.9	94.3	96.4	100	85.3	40.2	71.2	82.5
Zn/Total metals (%)	12.6	5.2	3.6	–	11.0	59.8	12.0	13.2
Pb/Total metals (%)	0.7	0.5	0	0	2.1	0	0	0
Zn/Cu ratio	0.15	0.06	0.04	0	0.13	1.49	0.17	0.16
P/Cu ratio					0.03	0.43	0.32	0.40

encountered in extended areas of the cross- section, above the first cuprite layer, as a consequence of the intense dezincification, which reaches its peak at this depth (Fig. 5). At the same time, the percentage of environmental elements reaches its minimum (Fig. 6). Therefore, the overall mass loss is determinant. The boundary of the original surface can be assigned at this depth. The irregular succession of a black layer and red cuprite layers of the DPL described above, can be associated with the complex mechanism of sulphides transformations to oxides described in [5]. Changes in volume have weakened the attachment scale and oxide subscale leading to fragmentation. The sulphur distribution testifies to that fact (Fig. 4). The corrosion products formed under anoxic conditions are no longer continuous and compact; they have been partially transformed after the establishment of continuous oxygen supply. It is also known that in the presence of turbulence, the adhered sulphide layers can be easily removed due to their pure mechanical stability [5]. In any case, after a certain period of burial, the aerobic corrosion processes have prevailed and this is evident by the oxygen map, not presented here, which is present across the entire layer stratification. The TM zone is characterized by morphological heterogeneity probably due to long

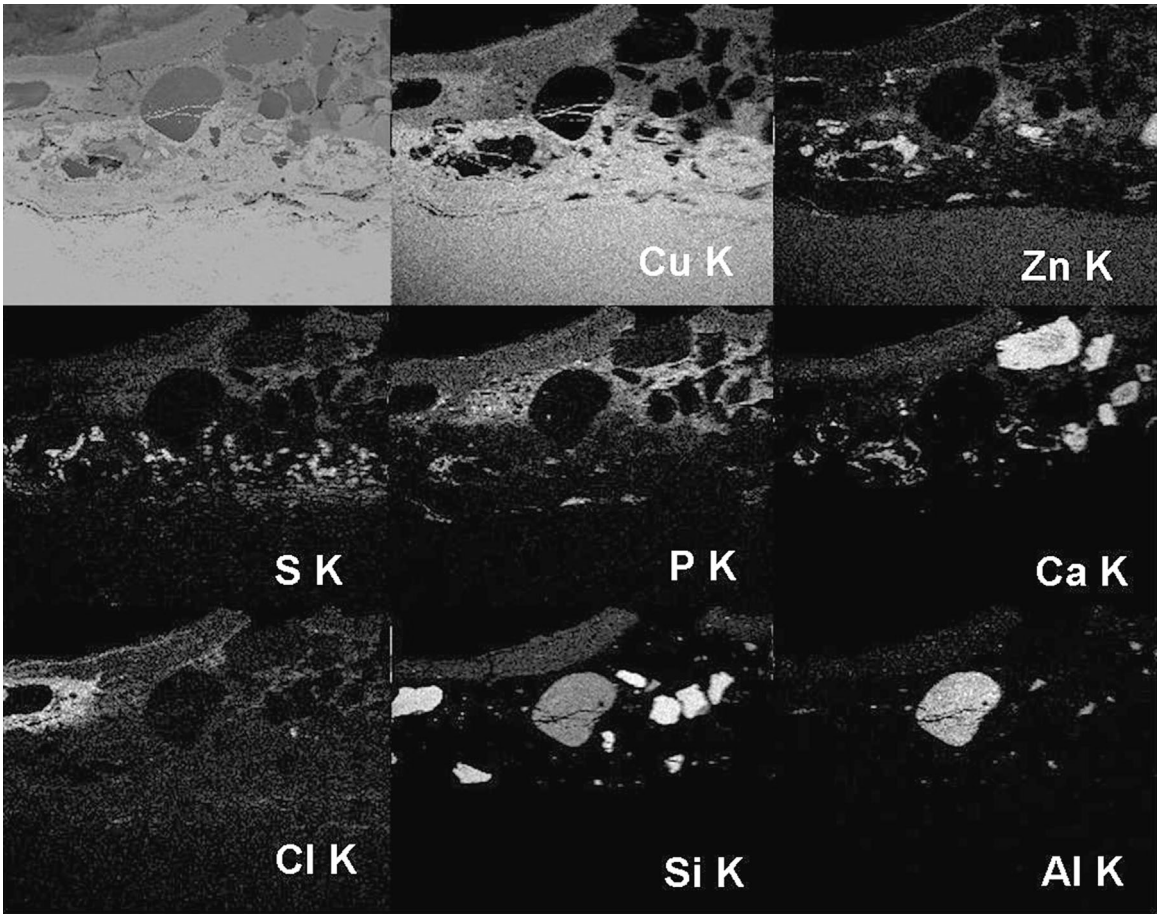

Figure 4. EDS elemental maps of copper, zinc, sulphur, phosphorus, calcium, chlorine, silicon and aluminium, of the art1 cross-section at a magnification x80.

Table 4. % elemental atomic concentrations detected by EDS spot analyses, at various depths of the corrosion layer stratification. The numbering corresponds to Figs. 3a and 3b. Here, presented together with the alloy composition.

Element	Alloy	1	2	3	4	5	6	7
C	0	6.0	8.2	11.8	14.3	11.9	25.0	5.1
O	0	39.1	27.4	2.5	57.7	62.5	50.5	55.9
Cu	85.9	51.5	63.5	58.8	23.4	6.5	4.4	0.0
Zn	12.6	1.9	0.0	0.0	3.0	9.6	0.7	0.0
Pb	0.7	0.0	0.0	0.0	0.6	0.0	0	0.0
Fe	0.8	0.0	0.0	0.0	0.4	0.0	1	0.4
Si	0	1.1	0.0	0.0	0.0	5.8	9.9	21.2
Cl	0	0.4	1.0	0.0	0.0	0.1	0.3	0.0
P	0	0.0	0.0	0.0	0.6	2.8	1.4	0.0
S	0	0.0	0.0	26.9	0.0	0.0	0	0.0
Na	0	0.0	0.0	0.0	0.0	0.0	0	1.0
Mg	0	0.0	0.0	0.0	0.0	0.0	2.7	1.0
Al	0	0.0	0.0	0.0	0.0	0.0	2.6	10.8
K	0	0.0	0.0	0.0	0.0	0.0	0.5	4.7
Ca	0	0.0	0.0	0.0	0.0	0.7	1.0	0.0

exposure in an aerated environment where many fluctuations in the surrounding microclimate conditions occurred. A huge red cuprite layer predominates (Fig. 2b), and a variety of cupric compounds such as malachite, vitreous bluish-green copper and zinc basic compounds have been accumulated and evolved towards the surface (Fig. 2b). The main characteristic is the high cuprous and cupric ions activity due to a gradual decuprification process depicted by copper mapping (Fig. 4). Copper cations diffuse across various directions - even across incorporated soil crystals (Fig. 3b). These diffusion paths produce fibrous structures of red, orange and yellow colours. Phosphorus mapping (Fig. 4) highlights an extended zone where phosphate compounds have been accumulated. This was an unusual finding, since their formation is difficult in aqueous environments. A Raman spectrum (Fig. 2c) was acquired from blue-green phosphate containing mineral phase, from the same area of spot 5 (Fig. 3b) that was also analyzed by EDS (Table 4). The low wavenumber region is presented without processing and background subtraction. A comparison with reference spectra of copper and zinc corrosion products was attempted [27–31]. Some correlations to basic copper phosphate minerals are possible. The spectrum was not sufficiently clear due to the complex nature of the sample and a direct comparison with the peak relative intensities of a pure compound is not indicative. Despite this fact, several bands are in agreement with pseudomalachite and ludjibaite spectra - also excited by a He-Ne laser of the same wavelength (632.8 nm) at 298K - reported by *Frost* [28]. These minerals are two crystalline polymorphs with the same chemical formula, which are very rarely reported as corrosion products. The stoichiometry and crystal system of the general group of copper phosphates is associated with the burial conditions. The relative stability of these minerals is determined by pH, the activity of cupric cations and the phosphate ion concentrations in soil [1].

Due to an intense fluorescence effect in the range of 4000 to 1000 cm^{-1} neither hydroxyl stretching vibrations nor antisymmetric stretching modes (ν_3) of phosphate anions could be observed. The symmetric stretching (ν_1), the symmetric bending (ν_2) and the out-of-plane bending modes (ν_4) of the phosphate group and the hydroxyl deformation modes can be detected together with some peaks that cannot be assigned with certainty. The peak at 999 cm^{-1} can be assigned to the ν_1 stretching vibration of pseudomalachite. The weak bands at 514 cm^{-1} and 475 cm^{-1} and the strong band at 647 cm^{-1} could be attributed to

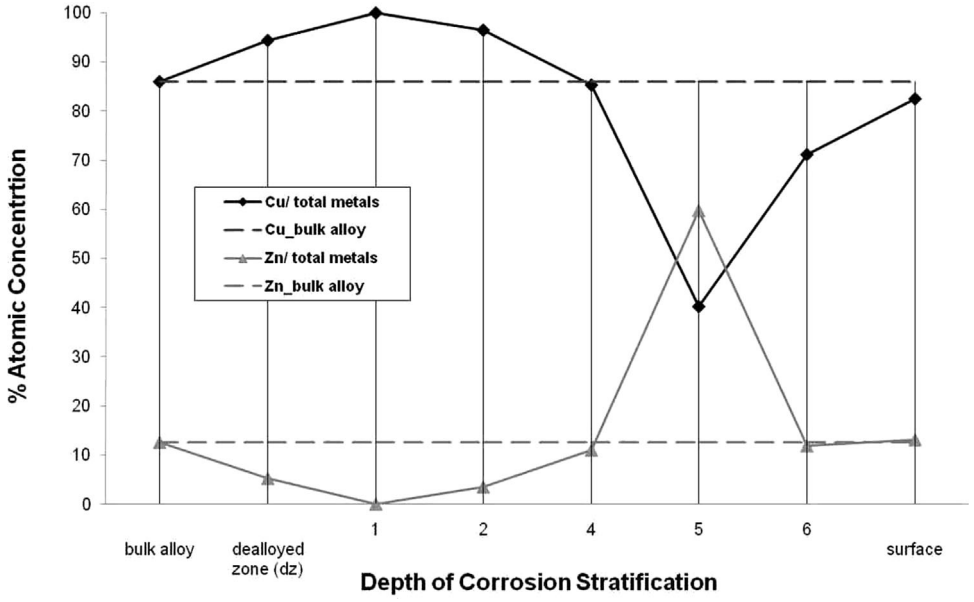

Figure 5. % Atomic percentages of major alloying elements (Cu and Zn), calculated from EDS spot chemical analyses, with respect to the bulk alloy composition. Numbering corresponds to Figs. 3a and 3b. The graph is based on the data of Table 3 and is indicative of the profile of dealloying processes which take place in the examined location of art1 cross-section.

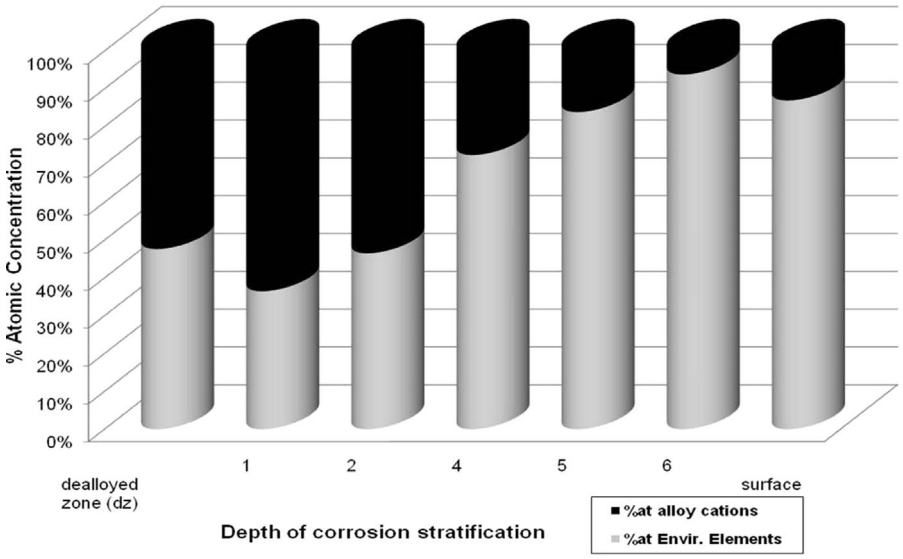

Figure 6. % relative atomic distribution of both alloying and environmental elements in various depths of the corroded cross-section of art1, calculated from EDS spot chemical analyses. The counterbalancing diffusion processes from and towards the metal core are being highlighted.

ν_4 modes, and match to several published spectra of ludjibaite and pseudomalachite [27,29]. The broad band at 809 cm^{-1} is possibly correlated with hydroxyl deformation vibrations. Peaks at 293 and 198 cm^{-1} appear slightly shifted compared to those of ludjibaite, at 298 and 195 cm^{-1}, respectively [29]. The significant concentration of zinc at the analyzed region, revealed by element mapping, allows the hypothesis that some zinc phosphates are also mixed with copper phosphates, since they exhibit Raman shifts in the same regions [28]. The substitution of copper by zinc in the crystal lattice of these corrosion products could not be excluded as well. The presence of a basic mixed copper-zinc carbonate in traces is another possible case. Rosasite, another bluish green mineral, exhibits Raman shifts at 1540, 508 and 193 cm^{-1} [30]. In the *art1* spectrum there are also weak peaks present at 1539, 514 and 197 cm^{-1}. No correlation with copper carbonates was found. It should be mentioned, that the calculated phosphorus/copper ratio of spot 5 (Table 3) is 0.43, very close to 0.40, which corresponds to the stoichiometry of ludjibaite and pseudomalachite. The chemical composition and shape of the incorporated grains is quite interesting. The analysis of spot 7 (Fig. 3b) shows that the large grain is potassium feldspar, most probably sanidine. Quartz and calcite were also identified by the element maps (Fig. 4). The rounded shape of the crystals is additional evidence that these materials are waterborne. Chlorine is detected at low concentration in the outer layers, distributing some local attacks with no further penetration (Fig. 4).

The EDS analyses of spots 4 to 6 (Fig. 3b) show a progressive increase in the percentage of the incorporated environmental elements (Fig. 6). The peak of copper migration outwards is observed at spot 5 (Fig. 3b) and then recedes. The compact mineral deposition prevents both zinc and copper cations to be released in soil. The outer mineral crust contains silicon and calcium (Fig. 4). The calculated zinc/copper atomic ratio at the surface reaches the value of the bulk alloy. The phosphorus/copper ratio at the surface matches with the ludjibaite and pseudomalachite stoichiometry.

From the relative observation of the two diffusion fronts (Fig. 6), one emerging from the alloying elements diffusion from the bulk alloy towards the surface and, the other one, corresponding to the environmental elements which diffuse towards the bulk metal, it is possible to conclude that after a certain period the corrosion processes were controlled by the anion vacancies transportation towards the bulk alloy, resulting in a corroded structure that can be regarded as Type II according to the *Robbiola* typology [3].

3.3.3 Bulk versus surface analysis - complementary results

Bulk elemental analyses were performed by both XRF and SEM/EDS. XRF has a penetration ability of a few hundreds of microns so can be used for bulk analyses. SEM/EDS penetration is less than 10 μm of material and can be used, theoretically, for surface layers and perhaps thin film analyses. In this particular case, given the unusual thickness of *art1* patina, and the uniform, well-developed external crust, the idea that EDS can serve the purposes of surface analysis seems quite reasonable in practice.

The EDS and XRF results are presented in Table 5. Carbon and oxygen, not measured by XRF, are also excluded from EDS quantification, in order to make a comparison between the results obtained by means of the two techniques. The concentration of incorporated silicon is higher than the one of

Table 5. % Elemental atomic concentrations detected by XRF bulk analysis and EDS surface analysis - normalized without oxygen and carbon.

	Cu	Zn	Fe	Pb	P	Cl	S	Si	Ca
EDS	40.6	6.5	2.1	0	16.3	2.8	0.7	15.4	9.7
XRF	61.2	16.2	5.0	0	1.7	4.1	0.2	5.6	4.1

calcium in both cases. Volcanic soils tend to have the greatest phosphorus sorption of all soils since volcanic soils contain large amounts of amorphous material [7]. This fact explains the rich phosphate patina of the examined object. Otherwise, the phosphates would have been washed away, as nitrates, and the precipitation of phosphate corrosion products would be extremely difficult in a non arid environment {1].

4 Conclusions

A corroded ancient metal fragment (*art1),* recovered after burial from Tiber riverbanks was studied. The chemical composition, the object shape and dimensions, as well as the structures of the metal core lead to the assumption that the examined fragment could be a part of an original brass medal or a large brass coin of the Roman Empire (most probably a sestertius). According to archaeological sources, its manufacture could be dated between the 1^{st} - 3^{rd} centuries AD. The suggested metallurgical treatments of the particular alloy, involve cold work after casting, annealing and subsequent cold work.

The sample has a complex and heterogeneous stratification, from a morphological and chemical point of view. The conducted analyses testify to the fact that the particular object has undergone a sequence of anaerobic and aerobic corrosion processes. The anoxic conditions are attributed to the biological activity of sulphate reducing bacteria. The sulphide layers have undergone subsequent transformations to copper oxides. The cross-section examination indicates: (a) an extensive dezincification process (selective dissolution of zinc), which is responsible for significant material loss near the border of the original surface, (b) a subsequent massive diffusion of environmental elements (such as oxygen, phosphate and carbonate anions, chlorides and soil elements) towards bulk metal that predominated over a decuprification process (transportation of copper cation vacancies) towards the surface. The gradual mineralization of the insoluble surface deposits stabilized the object and slowed down the migration processes. The most important parameters that explain the good preservation state of the brass artefact are the following: (a) the chlorine content was very low, (b) the presence of phosphates due to their sorption by volcanic soils created stable minerals and the pollution of river waters by fertilizers during the last decades did not altered the chemical context of the previous centuries and (c) the build up of the outer mineral crust has acted as a barrier to the migration processes.

Acknowledgments: The authors would like to express their gratitude to Dr. *Maria Perraki*, Assistant Professor at the Department of Geological Sciences, School of Mining Engineering and Metallurgy of National Technical University of Athens, for the Raman spectroscopy analyses and the valuable discussions. Special thanks to the researchers of the Archaeometry Laboratory, at National Centre for Scientific Research 'Demokritos' in Athens, Drs. *Y. Bassiakos, G. Mastrotheodoros* and *E. Filippaki*, for the EDS element mapping conducted at the SEM of their institute, their useful remarks and for their collaboration with the Lab of Physical Chemistry all these years.

5 References

[1] D. A. Scott, *Copper and Bronze in Art/Corrosion-Colorants-Conservation*, Getty Conservation Institute, Los Angeles **2002**.
[2] D. A. Scott, *Metallography and Microstructure of Ancient and Historic Metals*, Getty Conservation Institute in association with Archetype Books, Singapore, **1991**.
[3] L. Robbiola, J. M. Blengino, C. Fiaud, *Corros. Sci.*, **1998**, *40*, 2083.
[4] E. Mattsson, *Br. Corros. J.*, **1980**, *15*, 6.
[5] B. Little, P. Wagner, F. Mansfeld, *Int. Mater. Rev.*, **1991**, *36*, 253.
[6] M. B. McNeil, B. J. Little, *J. Am. Inst. Conserv.*, **1992**, *31*, 355.
[7] College of Tropical Agriculture and Human Resources -University of Hawaii Website: http://ctahr.hawaii.edu accessed in 27th February **2015**.
[8] F. Schweizer, presented at *Ancient and Historic Metals - Conservation & ScientificResearch (Symposium organized by the J. Paul Getty Museum and the Getty Conservation Institute)*, November **1991**, pp. 33–49.
[9] O. Oudbashi, S. M. Emami, H. Ahmadi, P. Davami, *Heritage Science*, **2013**, 1.
[10] G. M. Ingo, A. Bustamante, W. Alva, E. Angelini, R. Cesareo, E. Gigante, S. D. P. A. Zambrano, C. Riccucci, G. D. Carlo, E. I. Parisi, F. Faraldi, L. Chero, J. S. Fabian, *Appl. Phys. A: Mater. Sci. Process*, **2013**, *113*, 877.
[11] C. Riccucci, G. M. Ingo, A. Faustoferri, M. I. Pierigè, E. I. Parisi, G. Di Carlo, T. De Caro, F. Faraldi, *Appl. Phys. A: Mater. Sci. Process.*, **2013**, *113*, 959.
[12] F. Faraldi, A. Çilingiröglu, E. Angelini, C. Riccucci, T. DeCaro, A. Batmaz, A. Mezzo, D. Caschera, B. Cortese, *Appl. Phys. A: Mater. Sci. Process.*, **2013**, *113*, 911.
[13] D. A. Scott, *Stud. Conserv.*, **2005**, *50*, 179.
[14] N. Souissi, L. Bousselmi, S. Khosrof, E. Triki, *Mater. Corros.*, **2006**, *57*, 794.
[15] H. Hassairi, L. Bousselmi, E. Triki, G. M. Ingo, *Mater. Corros.*, **2007**, *58*, 121.
[16] O. Papadopoulou, J. Novakovic, P. Vassilliou, E. Filippaki, Y. Bassiakos, *Appl. Phys. A: Mater. Sci. Process.*, **2013**, *113*, 981.
[17] A. G. Nord, E. Mattsson, K. Tronner, *Prot. Met.*, **2005**, *41*, 309.
[18] M. Saheb, D. Neff, P. Dillmann, M. Descostes, H. Matthiesen, in: P. Dillmann, D. Watkinson, E. Angelini, A. Adriens (eds), *Corrosion and Conservation of Cultural Heritage Metallic Artifacts*, European Federation of CorrosionPublication, Number 65, Woodhead Publishing Limited, **2013**.
[19] A. N. Bear, G. Giordano, C. Giampaolo, R. A. F. Cas, *J. Volcanol. Geotherm. Res.*, **2009**, *83*, 183.
[20] S. Kempe, M. Pettine, G. Cauwet, *Biogeochemistry of European Rivers* in SCOPE 42 Bulletin, Scientific Committee on Problems of the Environment, **1991**.
[21] P. Kristensen, *Water quality of large rivers*, European Environment Agency, Denmark, **1996**.
[22] P.T. Craddock, *J. Archaeol. Sci.*, **1978**, *5*, 1.
[23] G. M. Ingo, T. De Caro, C. Riccucci, E. Angelini, S. Grassini, S. Balbi, P. Bernardini, D. Salvi, L. Bousselmi, A. Cilingiroglu, M. Gener, V. K. Gouda, O. Al Jarrah, S. Khosroff, Z. Mahdjoub, Z. Al Saad, W. El-Saddik, P. Vassiliou, *Appl. Phys. A: Mater. Sci. Process.*, **2006**, *83*, 513.

[24] G. M. Ingo, T. De Caro, C. Riccucci, S. Khosroff, *Appl. Phys. A: Mater. Sci. Process.*, **2006**, *83*, 581.
[25] G. F. Vander Voort, *ASM Metals Handbook*, Volume 9, ASM International, Materials Park **2004**, pp. 229–233.
[26] D. Neff, P. Dillmann, L. Bellot-Gurlet, C. Beranger, *Corros. Sci.*, **2005**, *47*, 515.
[27] R. L. Frost, T. Klorogge, P. A. Williams, W. Martens, T. E. Johnson, P. Leverett, *Spectrochim. Acta, Part A.*, **2002**, *58*, 2861.
[28] R. L. Frost, *Spectrochim. Acta, Part A.*, **2004**, *60*, 1439.
[29] R. L. Frost, P. A. Williams, W. Martens, P. Leverett, *J. Raman Spectrosc.*, **2002**, *33*, 260.
[30] R. L. Frost, *Spectrochim. Acta, Part A.*, **2003**, *59*, 22471.
[31] RRUFF Project Website: http://rruff.info accessed in 6th March 2015.

(Received: October 31, 2014) W8115
(Accepted: March 18, 2015)